



HAL
open science

Wavefront steering of elastic shear vertical waves in solids via a composite-plate-based metasurface

Jun Zhang, Xiaoshi Su, Yan Pennec, Yun Jing, Xiaofeng Liu, Ning Hu

► **To cite this version:**

Jun Zhang, Xiaoshi Su, Yan Pennec, Yun Jing, Xiaofeng Liu, et al.. Wavefront steering of elastic shear vertical waves in solids via a composite-plate-based metasurface. *Journal of Applied Physics*, 2018, 124 (16), pp.164505. 10.1063/1.5049515 . hal-03185618

HAL Id: hal-03185618

<https://hal.science/hal-03185618>

Submitted on 24 May 2022

HAL is a multi-disciplinary open access archive for the deposit and dissemination of scientific research documents, whether they are published or not. The documents may come from teaching and research institutions in France or abroad, or from public or private research centers.

L'archive ouverte pluridisciplinaire **HAL**, est destinée au dépôt et à la diffusion de documents scientifiques de niveau recherche, publiés ou non, émanant des établissements d'enseignement et de recherche français ou étrangers, des laboratoires publics ou privés.



Distributed under a Creative Commons Attribution 4.0 International License

Wavefront steering of elastic shear vertical waves in solids via a composite-plate-based metasurface

Cite as: J. Appl. Phys. **124**, 164505 (2018); <https://doi.org/10.1063/1.5049515>

Submitted: 23 July 2018 • Accepted: 08 October 2018 • Published Online: 25 October 2018

 Jun Zhang, Xiaoshi Su, Yan Pennec, et al.



View Online



Export Citation



CrossMark

ARTICLES YOU MAY BE INTERESTED IN

[Elastic metasurfaces for splitting SV- and P-waves in elastic solids](#)

Journal of Applied Physics **123**, 091701 (2018); <https://doi.org/10.1063/1.5007731>

[Asymmetric flexural wave transmission based on dual-layer elastic gradient metasurfaces](#)

Applied Physics Letters **113**, 183506 (2018); <https://doi.org/10.1063/1.5050671>

[Total-internal-reflection elastic metasurfaces: Design and application to structural vibration isolation](#)

Applied Physics Letters **113**, 221903 (2018); <https://doi.org/10.1063/1.5052538>

Lock-in Amplifiers
up to 600 MHz



Zurich
Instruments



Wavefront steering of elastic shear vertical waves in solids via a composite-plate-based metasurface

Jun Zhang,^{1,a)} Xiaoshi Su,² Yan Pennec,³ Yun Jing,⁴ Xiaofeng Liu,⁵ and Ning Hu^{1,b)}

¹College of Aerospace Engineering, Chongqing University, Chongqing 400044, China

²Mechanical and Aerospace Engineering, Rutgers University, Piscataway, New Jersey 08854, USA

³Institut d'Electronique, de Microelectronique et de Nanotechnologie (IEMN-UMR CNRS 8520), Université de Lille, Villeneuve d'Ascq, France

⁴Department of Mechanical and Aerospace Engineering, North Carolina State University, Raleigh, North Carolina 27695, USA

⁵The State Key Laboratory of Mechanical Transmissions, Chongqing University, Chongqing 400044, China

(Received 23 July 2018; accepted 8 October 2018; published online 25 October 2018)

We report a novel approach to control the wavefronts of shear vertical (SV) waves in solids using metasurfaces constituted by a stacked array of composite plates, which are composed of two connecting parts made of different materials. The metasurfaces are connected at two ends to the half-space solids where the elastic SV waves propagate. The incident SV waves in the left half-space solid induce flexural waves in the composite plates and subsequently are converted back to SV waves in the right half-space solid. The time delay of flexural waves in each composite plate of the metasurfaces is tuned through the varying length of the two connecting components. To quantitatively evaluate the time delay in each composite plate, a theoretical model for analyzing the phase of the transmitted SV waves is developed based on the Mindlin plate theory. To control the SV waves at will, each composite plate in the metasurface is delicately designed according to the proposed theoretical model. For illustrative purposes, two metasurfaces are designed and numerically validated. © 2018 Author(s). All article content, except where otherwise noted, is licensed under a Creative Commons Attribution (CC BY) license (<http://creativecommons.org/licenses/by/4.0/>).

<https://doi.org/10.1063/1.5049515>

I. INTRODUCTION

Controlling waves using artificial materials (e.g., metamaterials and metasurfaces) is a subject that has received substantial attention, since it has a multitude of applications in noise/vibration reduction, wave guiding, imaging, etc. To date, various controls in the form of cloaking,¹ negative refraction,^{2,3} non-reciprocal propagation,^{4–6} filtering,^{7–16} wave guiding,^{17–22} and other novel phenomena can be achieved.^{23–25} As reported in the past, two ways of controlling the wave exist: the active mode, through the employment of one or more physical fields,^{26–34} and the passive mode.

The dynamic behavior of thin plates has been well studied,³⁵ with such thin plates being generally employed as the basic mechanical elements in engineering. Consequently, the control of various elastic waves in thin plates has been explored.^{36–40} It is well known that the speed of flexural waves in thin plates not only is a function of material properties but also highly depends on the thickness of plates, which opens more opportunities for thin plates to control flexural and other waves. The cloaking of flexural waves in thin plates has been realized through several techniques, including the transformation method,^{36–38,41–43} the design of metamaterials,^{44,45} and active control using external sources.²⁷ Lamb-wave cloaking in thin plates was accomplished by Colombi *et al.*⁴⁰ through a beam-based resonant

metamaterial. In addition to cloaking, focusing³⁹ of flexural waves in thin plates was also studied through a rational selection of the thickness profile of thin plates. Based on the fact that the speed of flexural waves is dependent on the thickness of thin plates, the isolation of vibration for a circular area in thin plates was realized by Climente *et al.*⁴⁶ Chen *et al.*⁴⁷ proposed a transformation technique to design waveguides for flexural waves in thin plates and implemented them through active elastic metamaterials. In summary, the study of the control of flexural waves and Lamb waves in thin plates has been extensively conducted. Readers are referred to the review by Zhu *et al.*⁴⁸ for more details.

Thin plates are also capable of manipulating the waves coming from outside that are not flexural or Lamb waves. For example, Su *et al.*⁴⁹ designed a plate-based device to realize focusing, refraction, and asymmetric transmission of elastic waves in solids. Inspired by this work, we proposed a high-quality narrow passband filter for elastic shear vertical (SV) waves.^{15,16} Recently, the idea proposed by Su *et al.*⁴⁹ was utilized by the same authors to devise a splitter for elastic SV and P waves in solids.⁵⁰ This splitter was designed by introducing an array of aligned cracks in a bulky solid to yield many thin plates of different thicknesses. The thickness of each plate in the splitter is delicately chosen according to the generalized Snell's law⁵¹

$$(\sin \theta_t - \sin \theta_i)k_T = \frac{d\Phi}{dy}, \quad (1)$$

where k_T denotes the wavenumber of the SV wave in the

^{a)}mejzhang@cqu.edu.cn

^{b)}ninghu@cqu.edu.cn



solid, Φ the phase of the transmitted wave, and θ_i and θ_t the incident and transmitted angles, respectively. The underlying physics behind this splitter is that SV waves in solids induce flexural waves in the thin plates, while there is no mode conversion between solids and thin plates for P waves. While the phase velocity of flexural waves is sensitive to the thickness of each plate, the thickness does not affect the speed of P waves. Consequently, the thickness h of the thin plates was chosen as the variable to tune the speed of flexural waves to further control the SV waves in solids.

In this work, instead of the thickness h , the material properties of the thin plates are chosen to manipulate the speed of flexural waves. To control the elastic SV waves in solids, the thin plates in the splitter designed by Su *et al.*⁵⁰ are replaced by composite plates of an identical thickness. The composite plates are composed of two connecting parts made of different materials. When the total length of the composite plate is fixed, the time delay of flexural waves through it can be tuned by different combinations of the two parts. The metasurface with a specific function can be designed based on the rational selection of the composite plates. In particular, such a study can be useful for Micro-Electro-Mechanical System (MEMS) structures in which solid plates are the typical components supported by solid media and for which specific waves, e.g., elastic SV waves, should be controlled at certain frequency ranges.

The rest of this paper is organized as follows: The design of the metasurfaces and the transmission properties of the unit cell are introduced and analyzed in Sec. II with an emphasis on the phase modulation of the transmitted SV waves by the varying length of the two connecting components of the composite plates. Two metasurfaces are designed and numerically verified using full finite-element-method (FEM) simulations to examine the proposed approach in Sec. III. Conclusions are presented in Sec. IV.

II. DESIGN OF METASURFACES AND TRANSMISSION PROPERTIES

A. Description of metasurfaces

Figure 1 is a two-dimensional (2D) schematic of the metasurfaces consisting of parallel separated thin composite plates connected at two ends to the half-space solids. The thickness and the total length of the composite plates are denoted as h and l , respectively, and the gap between two adjacent plates is a , which is assumed to be considerably smaller than h . All the composite plates are composed of two kinds of materials, denoted as materials 1 and 2, respectively. In this work, aluminum is selected as material 1 with Young's modulus $E = 70$ GPa, mass density $\rho = 2700$ kg/m³, and Poisson's ratio $\nu = 0.33$. Material 2 is a platonic material with a higher Young's-modulus-to-mass-density ratio, with detailed properties of $E = 500$ GPa, $\rho = 2000$ kg/m³, and $\nu = 0.31$. In fact, carbon-fiber-reinforced composite is a potential candidate for material 2. In principle, other materials can also be used as material 2, provided that it has a higher Young's-modulus-to-mass-density ratio in contrast to material 1. The length ratio of the two connecting parts of

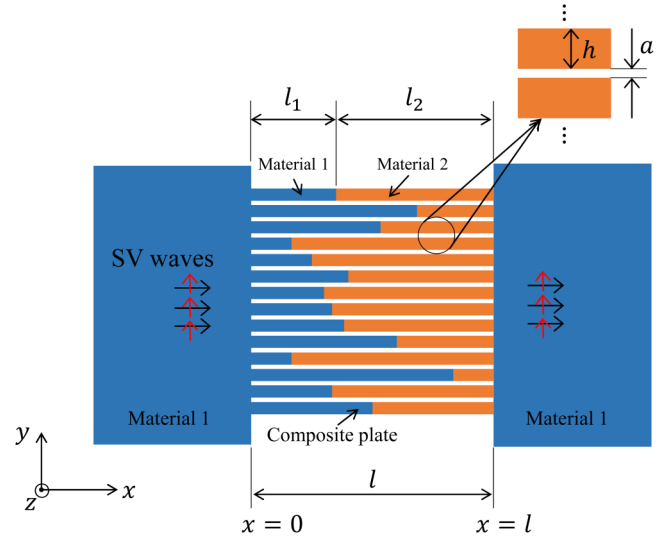


FIG. 1. 2D schematic of the metasurfaces made by aligned parallel thin composite plates connected at two ends to the half-space solids. Different colors represent different materials.

the composite plates, l_1/l_2 , is defined as α , which varies from 0 to 1, representing various composite plates. As illustrated by the short arrows in Fig. 1, the horizontal direction indicates the propagation of SV waves, while the vertical direction indicates the vibration of material particles. Strictly speaking, the proposed structure in Fig. 1 is more like a metamaterial, and it may not qualify as a metasurface due to its relatively large thickness. However, the authors refer it as a metasurface since its role is similar to those of the metasurfaces for wavefront manipulation.

B. Governing equations for flexural waves in thin plates

In Mindlin plate theory,⁵⁰ the governing equation for flexural waves in the plate with thickness h , and without any external loading, is expressed as

$$\begin{aligned} \mu\chi \left(\frac{\partial^2 w}{\partial x^2} - \frac{\partial \psi}{\partial x} \right) - \rho \frac{\partial^2 w}{\partial t^2} &= 0, \\ D \frac{\partial^2 \psi}{\partial x^2} + \chi\mu \left(\frac{\partial w}{\partial x} - \psi \right) h - \lambda \frac{\rho h^3}{12} \frac{\partial^2 \psi}{\partial t^2} &= 0, \end{aligned} \quad (2)$$

where $w(x, t)$ is the out-of-plane displacement field of the

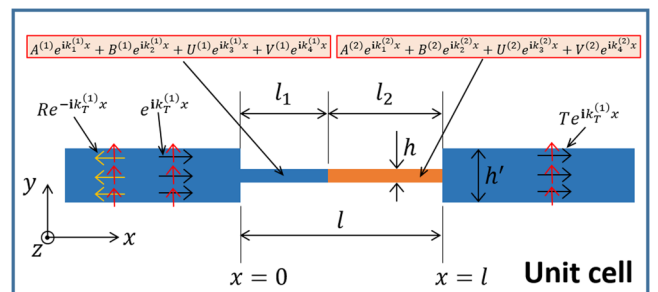


FIG. 2. Unit cell used to analyze the transmission spectrum of elastic SV waves through composite plates in designed metasurfaces.

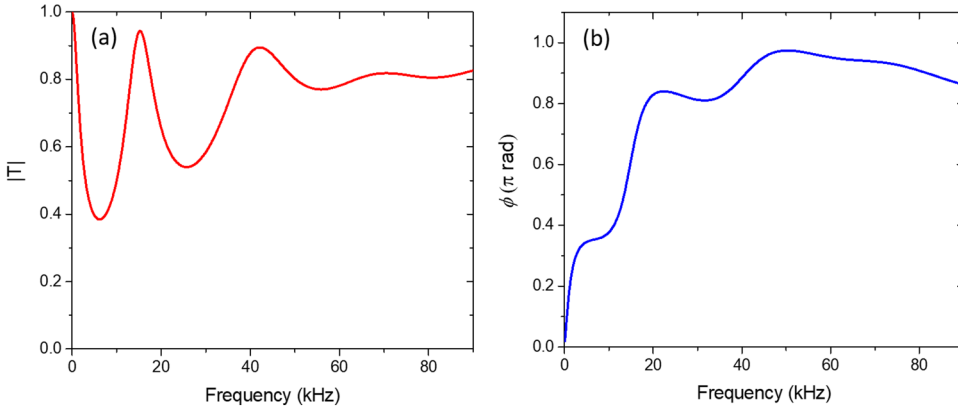


FIG. 3. Theoretical (a) magnitudes and (b) phases of the transmitted waves changing with frequencies.

neutral plane and $\Psi(x, t)$ is the bending angle. μ is the shear modulus and $D = Eh^3/12(1 - \nu^2)$ the bending stiffness of the plate, and χ and λ are the shear and inertia correction factor, respectively. In this work, χ and λ are set as

$$\begin{cases} \chi = \frac{20}{17 - 7\nu} \left[1 + \sqrt{1 - \frac{200(1 - \nu)}{\chi_0(17 - 7\nu)^2}} \right]^{-1}, \\ \lambda = \chi/\chi_0, \end{cases} \quad (3)$$

with $\chi_0 = \pi^2/12$, according to the recent work by Norris.⁵² General solutions to Eq. (2) can be expressed in the forms $w(x, t) = We^{i(kx - \omega t)}$ and $\Psi(x, t) = \Psi e^{i(kx - \omega t)}$, where i denotes the imaginary unit. Substituting the above expressions for the out-of-plane displacements and bending angles into Eq. (2) yields

$$\begin{pmatrix} \rho\omega^2 - \mu\chi k^2 & -i\mu\chi k \\ i\mu\chi kh & \lambda \frac{\rho h^3}{12} \omega^2 - Dk^2 - \chi\mu h \end{pmatrix} \begin{pmatrix} W \\ \Psi \end{pmatrix} = \mathbf{0}. \quad (4)$$

The equation for the wavenumber k is

$$k^4 - \left(\frac{k_T^2}{\chi} + \lambda k_P^2 \right) k^2 + \frac{\lambda k_T^2 k_P^2}{\chi} - k_F^4 = 0, \quad (5)$$

with $k_P = \omega\sqrt{\rho(1 - \nu^2)}/E$, $k_T = \omega\sqrt{\rho}/\mu$, and $k_F = (\rho h \omega^2/D)^{1/4}$ representing the wave numbers of the longitudinal and transverse waves in 2D plane-strain problems and the flexural waves in the plates, respectively. Four solutions for k are calculated as

$$\begin{aligned} k_{1,2} &= \pm \left\{ \frac{1}{2} \left(\frac{k_T^2}{\chi} + \lambda k_P^2 \right) + \sqrt{\frac{1}{4} \left(\frac{k_T^2}{\chi} - \lambda k_P^2 \right)^2 + k_F^4} \right\}^{1/2}, \\ k_{3,4} &= \pm \left\{ \frac{1}{2} \left(\frac{k_T^2}{\chi} + \lambda k_P^2 \right) - \sqrt{\frac{1}{4} \left(\frac{k_T^2}{\chi} - \lambda k_P^2 \right)^2 + k_F^4} \right\}^{1/2}, \end{aligned} \quad (6)$$

where $k_{1,2}$ are always real and correspond to traveling waves; however, $k_{3,4}$ are imaginary as $\omega < \frac{1}{h} \sqrt{12\mu\chi/\lambda\rho}$ and correspond to evanescent waves.

C. Transmission of SV waves through composite plates in metasurfaces

To obtain the transmission spectrum of elastic SV waves through the composite plates in the designed metasurfaces, a unit cell as proposed in Refs. 16, 49, and 50 is adopted as shown in Fig. 2. Under a normal incidence of a plane elastic SV wave, the wave fields in the unit cell can be expressed as

$$W(x) = \begin{cases} e^{ik_r^{(1)}x} + R e^{-ik_r^{(1)}x}, & x < 0, \\ A^{(1)} e^{ik_1^{(1)}x} + B^{(1)} e^{ik_2^{(1)}x} + U^{(1)} e^{ik_3^{(1)}x} + V^{(1)} e^{ik_4^{(1)}x}, & 0 < x < l_1, \\ A^{(2)} e^{ik_1^{(2)}x} + B^{(2)} e^{ik_2^{(2)}x} + U^{(2)} e^{ik_3^{(2)}x} + V^{(2)} e^{ik_4^{(2)}x}, & l_1 < x < l, \\ T e^{ik_T^{(1)}x}, & x > l, \end{cases} \quad (7)$$

where R , $A^{(i)}$, $B^{(i)}$, $U^{(i)}$, $V^{(i)}$, ($i = 1, 2$), and T are the unknown coefficients. Superscripts (1) and (2) indicate quantities associated with materials 1 and 2, respectively. The above 10 unknowns are determined by the continuity of out-of-plane displacements, bending angles, average shear forces at locations $x = 0, l_1$, and l , and bending moments at $x = l_1$. The

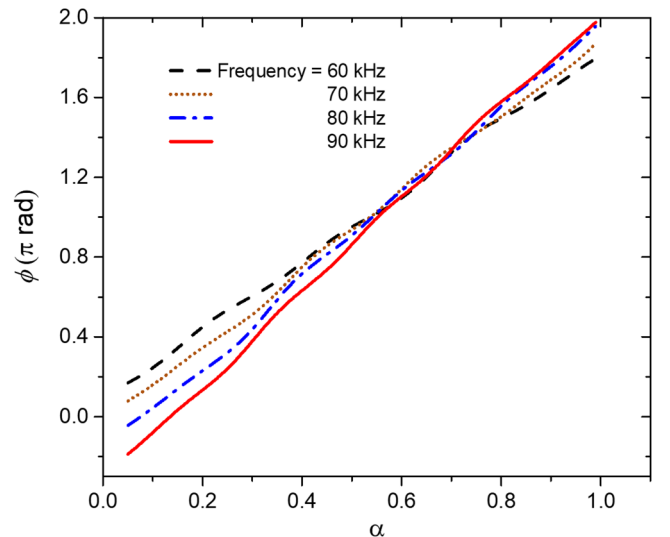


FIG. 4. Theoretical phases of the transmitted waves changing with α at four different frequencies. $h = 5$ mm, $l = 5$ cm, and $a = 0.5$ mm throughout the paper.

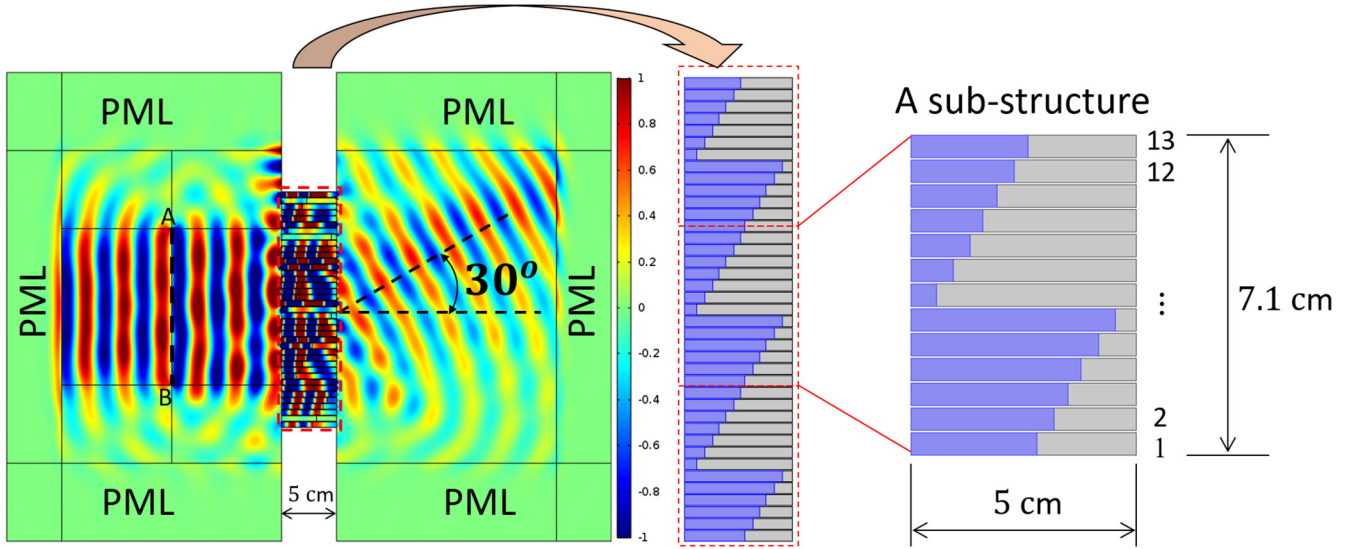


FIG. 5. Simulated curl of the displacement field at 90 kHz normalized by the incident wave, with detailed structure of designed refraction lens.

bending angle in the half-space solids is calculated as $\Psi = \frac{\partial W}{\partial x}$, and the corresponding value in the plate is related to the out-of-plane displacement in the form of

$$\psi = \frac{\rho\omega^2 - \mu\chi k^2}{i\mu\chi k} W. \quad (8)$$

The average shear forces in the half-space solids are $Q = \mu h' \frac{\partial W}{\partial x}$ and $Q = \mu\chi h \left(\frac{\partial W}{\partial x} - \Psi \right)$ in the plate, where $h' = h + a$. The bending moment in the plate is $M = D \frac{\partial \Psi}{\partial x}$. Therefore, the equations governing the 10 unknowns can be established. Solving this system yields the unknowns.

Figure 3 shows the theoretical magnitudes and phases of the transmitted waves at different frequencies for the case $h = 5$ mm, $l = 50$ mm, $a = 0.5$ mm, and $\alpha = 0.5$. The results indicate that the transmission efficiency of the current design is acceptable at relatively high frequencies.

The influence of α on the phase of the transmitted waves at four frequencies is illustrated in Fig. 4. It is evident that α can be taken as an effective means by which to tune the phase of the transmitted waves from 0 to 2π , particularly at higher frequencies. Therefore, according to the generalized Snell's law, it is possible that the elastic SV waves can be controlled by α .

III. APPLICATIONS

As an illustration of the applications of the above design, we present two numerical experiments. One was conducted with the design of a planar refraction lens for plane SV waves and the other with the design of a converter for the shape of wavefronts of SV waves from a plane to a cylindrical surface.

A. Planar refraction lens for elastic SV waves in solids

A planar refraction lens for normal incident elastic SV waves propagating in solids was designed at 90 kHz. As an example, the angle of the refracted wave transmitted through this lens was set as 30° . To achieve this, three identical sub-structures were used in this lens, as represented by the dashed rectangles in Fig. 5. Each sub-structure is composed of 13 composite plates that are selected from the phase of the transmitted waves versus the α curve presented in Fig. 4. The 13 composite plates are numbered from bottom to top in each sub-structure with a total thickness of 7.1 cm, as shown in Fig. 5. The detailed parameters for the 13 composite plates are tabulated in Table I.

To examine the performance of the designed lens, a series of full numerical simulations using COMSOL® MultiPhysics software were conducted. The numerical model is plotted in Fig. 5, where the blue color represents material 1 and the gray color material 2. The perfectly matched layers (PMLs) are employed at the external zone

TABLE I. Parameters of the 13 composite plates constituting the lens of a refraction angle of 30° at 90 kHz.

Plate	α	$\Phi(\pi)$	$ T $
1	0.5588	1.0000	0.8217
2	0.6352	1.1586	0.7972
3	0.6967	1.3171	0.8188
4	0.7545	1.4757	0.7686
5	0.8328	1.6342	0.7549
6	0.9073	1.7928	0.8554
7	0.1134	1.9513	0.8203
8	0.1879	0.1099	0.8004
9	0.2625	0.2684	0.8374
10	0.3184	0.4270	0.8303
11	0.3817	0.5855	0.7457
12	0.4582	0.7441	0.7737
13	0.5197	0.9027	0.8368

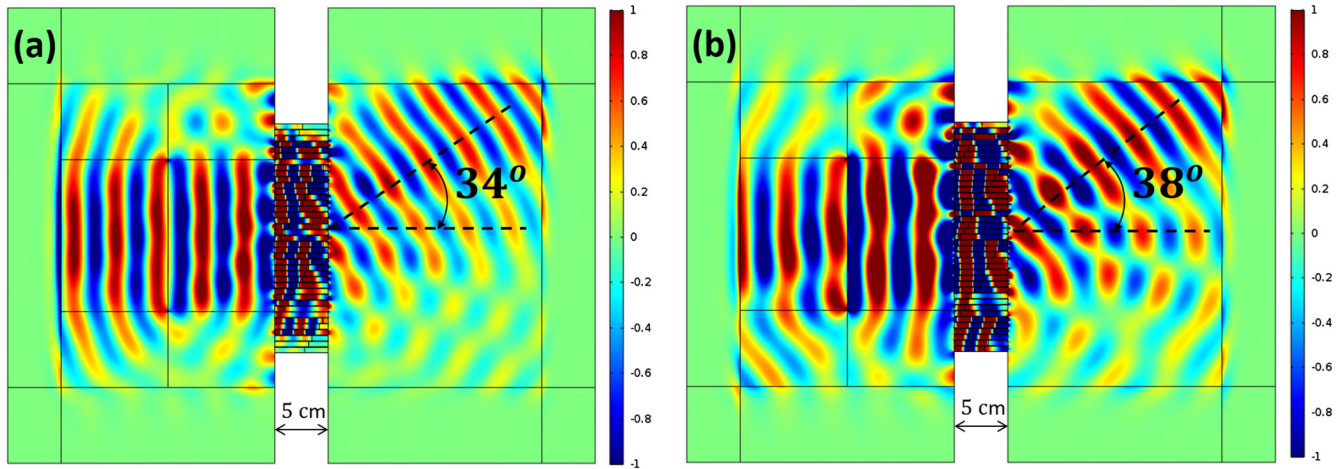


FIG. 6. Simulated normalized curl of displacement field at (a) 80 and (b) 70 kHz for designed planar refraction lens.

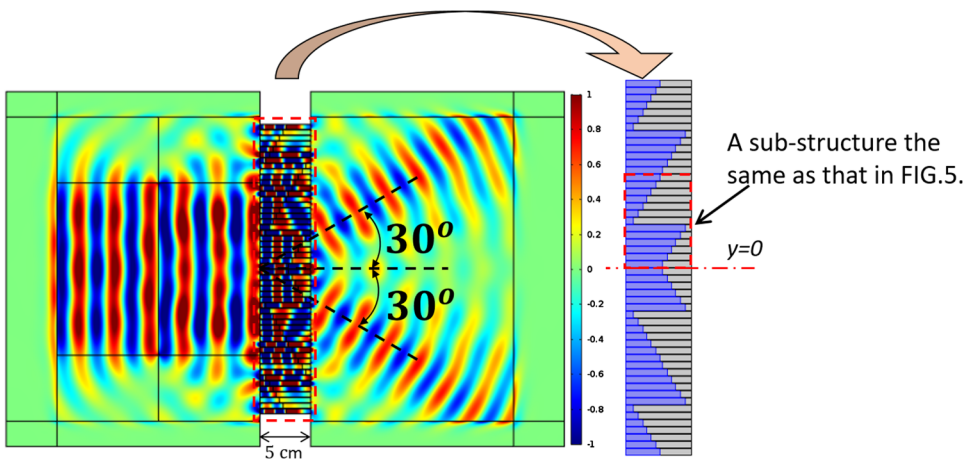


FIG. 7. Simulated normalized curl of displacement field for the designed splitter for plane SV waves propagating in solids at 90 kHz; the inset shows the splitter structure.

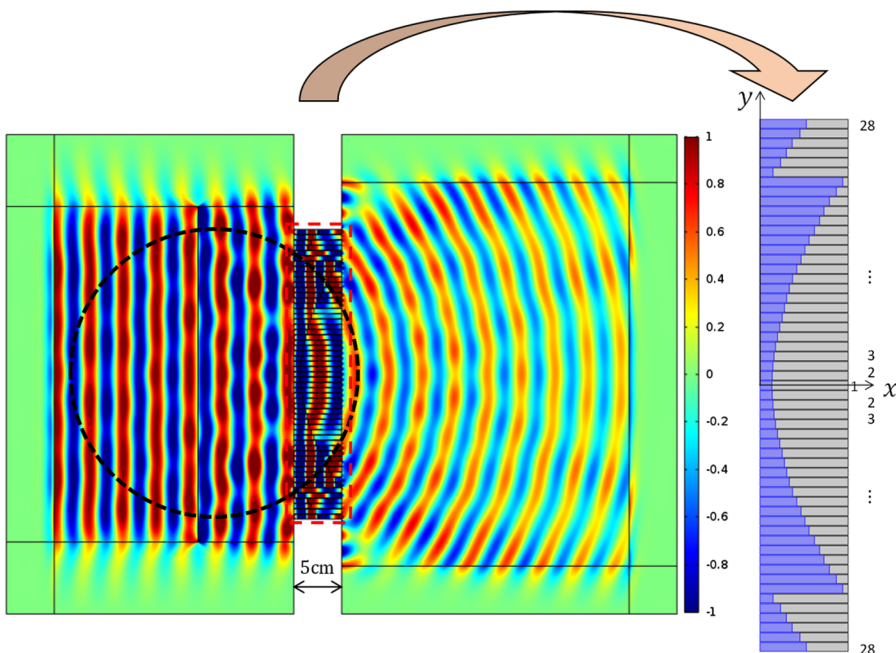


FIG. 8. Simulated normalized curl of displacement field for a designed converter of wavefronts at 90 kHz; the inset shows the structure of the designed converter.

to yield non-reflecting boundaries. A uniform vertical displacement of a unit magnitude is applied on the dashed line AB to generate a plane SV wave. The simulated displacement fields at 90 kHz are illustrated in Fig. 5. The results show that the refracted wave is indeed at an angle of 30° with respect to the incident wave, which is in good agreement with the theoretically prescribed value. Although this lens was designed only for the single frequency of 90 kHz, numerical simulations were also conducted at other frequencies, i.e., 80 and 70 kHz, and the results are illustrated in Fig. 6. The results show that the angle of the refracted wave is approximately 34° at 80 kHz and 38° at 70 kHz, and both are slightly different from the predicted angle, i.e., 30° . It can be concluded that, although this lens was designed to work at a single frequency, it actually works reasonably well in a range of frequencies centered on the design frequency.

As a further application, Fig. 7 shows the simulated curl of the displacement field for a designed wave-splitting lens. As shown in the inset, in this lens, four sub-structures are employed. Two sub-structures are located just above $y=0$, which possess the same properties of the sub-structure shown in Fig. 5 and Table I. In addition, other two sub-structures are located symmetrically about $y=0$. The results indicate that the incident SV wave is split into two parts with the propagation directions symmetric about the $y=0$ axis.

B. Converter of shape of wavefronts for SV waves

We designed a converter to convert the shape of wavefronts for elastic SV waves in solids from planes to cylindrical surfaces. The required phase profile along the vertical direction is described as Eq. (19) in Ref. 50. In this work, as shown in the inset of Fig. 8, 28 composite plates were selected from the curve at 90 kHz as presented in Fig. 4. Table II lists the detailed parameters of these 28 plates. Similarly, a series of full numerical simulations were performed. It is noted that, in the numerical simulations, another 27 plates, except for plate 1, were symmetrically distributed about $y=0$. Figure 8 shows the simulated normalized curl of the displacement field at 90 kHz, for a comparison, on which

TABLE II. Parameters of the 28 composite plates constituting the converter at 90 kHz.

Plate	α	$\Phi(\pi)$	$ T $
1	0.1348	0	0.8179
2	0.1387	0.0087	0.8167
3	0.1467	0.0261	0.8139
4	0.1592	0.0522	0.8088
5	0.1763	0.0869	0.8027
6	0.1986	0.1301	0.8002
7	0.2247	0.1817	0.8091
8	0.2513	0.2416	0.8287
9	0.2773	0.3098	0.8458
10	0.3038	0.3860	0.8434
11	0.3330	0.4700	0.8110
12	0.3696	0.5618	0.7581
13	0.4176	0.6612	0.7362
14	0.4665	0.7680	0.7851
15	0.5103	0.8819	0.8336
16	0.5571	1.0028	0.8229
17	0.6176	1.1306	0.7936
18	0.6764	1.2649	0.8166
19	0.7268	1.4055	0.8001
20	0.7888	1.5524	0.7407
21	0.8673	1.7052	0.8002
22	0.9393	1.8638	0.8856
23	0.1475	0.0279	0.8135
24	0.2321	0.1974	0.8138
25	0.2989	0.3721	0.8459
26	0.3653	0.5518	0.7635
27	0.4530	0.7362	0.7668
28	0.5263	0.9253	0.8372

a dashed circle is also plotted. As we can see, the shape of the wavefront of the SV wave is changed from a plane to a perfect cylindrical surface. As before, although this converter is designed at a single frequency, the numerical results at 80 and 70 kHz illustrated in Fig. 9 indicate that this converter actually also works well in a range of frequencies around the design frequency. In addition, as seen in Fig. 8, the circular fringes present a variation in their amplitude. Such a variation can be understood by the shift of the Fabry-Pérot resonances

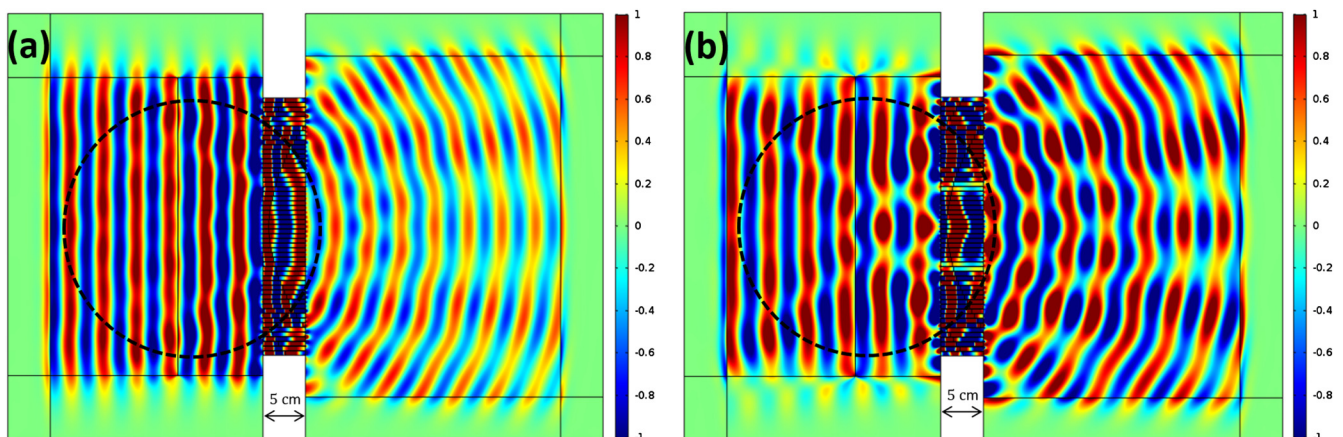


FIG. 9. Simulated normalized curl of displacement field at (a) 80 and (b) 70 kHz for a designed converter.

inside the slits that leads to different levels of transmission at their exits. It is worth mentioning that when the composite plates are selected according to Eq. (19) in Ref. 50 with an addition of a minus sign to the right-hand side, focusing on plane SV waves can be realized.

IV. CONCLUSIONS

In conclusion, we have proposed an approach for controlling elastic SV waves in solids using metasurfaces made of composite plates. The composite plates were made of two connecting parts with different materials. A theoretical model based on the Mindlin plate theory was developed to evaluate the transmission of elastic SV waves through such a composite plate. The theoretical results indicate that the phase of the transmitted waves can be tuned between 0 and 2π through the length change of the connecting two parts, which indicates that the proposed composite plates are able to steer elastic SV waves effectively. To examine the performance of the proposed idea of steering elastic SV waves using the composite plates, two numerical experiments were conducted. One used the design of a planar refraction lens for elastic SV waves in solids and the other the design of a converter to convert the shape of wavefronts for SV waves from planes to cylindrical surfaces. The full numerical simulations successfully verified the two designs. In addition to these two illustrative applications, this idea also benefits other applications, such as non-reciprocal propagation of SV waves with the combination of phononic crystals.

ACKNOWLEDGMENTS

This work was supported by the National Natural Science Foundation of China (NNSFC) (Grant Nos. 11502036 and 11632004). The Key Program for International Science and Technology Cooperation Projects of the Ministry of Science and Technology of China (No. 2016YFE0125900), the Guangxi Key Laboratory of Manufacturing Systems and Advanced Manufacturing Technology (No. 16-380-12-014k), and the Key Project of Natural Science Foundation of CQ CSTC (No. cstc2017jcyjBX0063) also provided partial financial support.

- ¹J. B. Pendry, D. Schurig, and D. R. Smith, *Science* **312**(5781), 1780 (2006).
- ²J. B. Pendry, *Phys. Rev. Lett.* **85**(18), 3966 (2000).
- ³C. Shen, Y. Xie, N. Sui, W. Wang, S. A. Cummer, and Y. Jing, *Phys. Rev. Lett.* **115**(25), 254301 (2015).
- ⁴X. F. Li, X. Ni, L. A. Feng, M. H. Lu, C. He, and Y. F. Chen, *Phys. Rev. Lett.* **106**(8), 084301 (2011).
- ⁵H. Nassar, X. C. Xu, A. N. Norris, and G. L. Huang, *J. Mech. Phys. Solids* **101**, 10 (2017).
- ⁶B. Liang, B. Yuan, and J. C. Cheng, *Phys. Rev. Lett.* **103**(10), 104301 (2009).
- ⁷A. Khelif, P. A. Deymier, B. Djafari-Rouhani, J. O. Vasseur, and L. Dobrzynski, *J. Appl. Phys.* **94**(3), 1308 (2003).
- ⁸Y. Pennec, B. Djafari-Rouhani, J. O. Vasseur, A. Khelif, and P. A. Deymier, *Phys. Rev. E* **69**(4), 046608 (2004).
- ⁹P. Zhang and A. C. To, *Appl. Phys. Lett.* **102**(12), 121910 (2013).
- ¹⁰I. K. Lee, H. M. Seung, and Y. Y. Kim, *J. Sound Vib.* **355**, 86 (2015).
- ¹¹H.-W. Dong, Y.-S. Wang, and C. Zhang, *Ultrasonics* **76**, 109 (2017).
- ¹²Y. Pennec, B. Djafari-Rouhani, J. O. Vasseur, H. Larabi, A. Khelif, A. Choujaa, S. Benchabane, and V. Laude, *Appl. Phys. Lett.* **87**(26), 141 (2005).

- ¹³R. P. Moiseyenko, Y. Pennec, R. Marchal, B. Bonello, and B. Djafari-Rouhani, *Phys. Rev. B* **90**(13), 134307 (2014).
- ¹⁴Y. Pennec, B. Djafari-Rouhani, H. Larabi, A. Akjouj, and G. Leveque, *New J. Phys.* **14**, 073039 (2012).
- ¹⁵J. Zhang, L. H. Zeng, C. L. Hu, W. S. Yan, Y. Pennec, and N. Hu, *AIP Adv.* **8**(3), 035323 (2018).
- ¹⁶J. Zhang, Y. Liu, W. Yan, and N. Hu, *AIP Adv.* **7**, 085318 (2017).
- ¹⁷Y. Xie, W. Wang, H. Chen, A. Konneker, B.-I. Popa, and S. A. Cummer, *Nat. Commun.* **5**, 5553 (2014).
- ¹⁸Y. Li, G. Yu, B. Liang, X. Zou, G. Li, S. Cheng, and J. Cheng, *Sci. Rep.* **4**, 6830 (2014).
- ¹⁹W. Wang, Y. Xie, A. Konneker, B.-I. Popa, and S. A. Cummer, *Appl. Phys. Lett.* **105**(10), 101904 (2014).
- ²⁰Y. Li, B. Liang, X. Tao, X.-f. Zhu, X.-y. Zou, and J.-c. Cheng, *Appl. Phys. Lett.* **101**(23), 233508 (2012).
- ²¹Y. Li, X. Jiang, R.-q. Li, B. Liang, X.-y. Zou, L.-l. Yin, and J.-c. Cheng, *Phys. Rev. Appl.* **2**(6), 064002 (2014).
- ²²J. Mei and Y. Wu, *New J. Phys.* **16**, 123007 (2014).
- ²³Y. Li, C. Shen, Y. Xie, J. Li, W. Wang, S. A. Cummer, and Y. Jing, *Phys. Rev. Lett.* **119**(3), 035501 (2017).
- ²⁴Y. Xie, C. Shen, W. Wang, J. Li, D. Suo, B.-I. Popa, Y. Jing, and S. A. Cummer, *Sci. Rep.* **6**, 35437 (2016).
- ²⁵Y. Zhu, X. Fan, B. Liang, J. Cheng, and Y. Jing, *Phys. Rev. X* **7**(2), 021034 (2017).
- ²⁶X. Chen, X. Xu, S. Ai, H. Chen, Y. Pei, and X. Zhou, *Appl. Phys. Lett.* **105**(7), 071913 (2014).
- ²⁷G. Futhazar, W. J. Parnell, and A. N. Norris, *J. Sound Vib.* **356**, 1 (2015).
- ²⁸R. Zhu, Y. Y. Chen, M. V. Barnhart, G. K. Hu, C. T. Sun, and G. L. Huang, *Appl. Phys. Lett.* **108**(1), 011905 (2016).
- ²⁹Y. Y. Chen, G. K. Hu, and G. L. Huang, *Smart Mater. Struct.* **25**(10), 105036 (2016).
- ³⁰E. A. Flores Parra, A. Bergamini, B. Van Damme, and P. Ermanni, *Appl. Phys. Lett.* **110**(18), 184103 (2017).
- ³¹T. Yang, Z.-G. Song, E. Clerkin, Y.-W. Zhang, J.-H. Sun, Y.-S. Su, L.-Q. Chen, and P. Hagedorn, *AIP Adv.* **7**(9), 095323 (2017).
- ³²A. Baz, *New J. Phys.* **11**, 123010 (2009).
- ³³Y. Y. Chen, G. L. Huang, and C. T. Sun, *J. Vib. Acoust.* **136**(6), 061008 (2014).
- ³⁴X. Li, Y. Chen, G. Hu, and G. Huang, *Smart Mater. Struct.* **27**(4), 045015 (2018).
- ³⁵C. Mei and B. R. Mace, *J. Vib. Acoust.* **127**(4), 382 (2005).
- ³⁶M. Brun, D. J. Colquitt, I. S. Jones, A. B. Movchan, and N. V. Movchan, *New J. Phys.* **16**, 093020 (2014).
- ³⁷D. J. Colquitt, M. Brun, M. Gei, A. B. Movchan, N. V. Movchan, and I. S. Jones, *J. Mech. Phys. Solids* **72**, 131 (2014).
- ³⁸A. Zareei and M. R. Alam, *Phys. Rev. E* **95**(6), 063002 (2017).
- ³⁹G. Lefebvre, M. Dubois, R. Beauvais, Y. Achaoui, R. K. Ing, S. Guenneau, and P. Sebbah, *Appl. Phys. Lett.* **106**(2), 024101 (2015).
- ⁴⁰A. Colombi, P. Roux, S. Guenneau, and M. Rupin, *J. Acoust. Soc. Am.* **137**(4), 1783 (2015).
- ⁴¹Y. Liu, Z. Ma, and X. Su, *J. Acoust. Soc. Am.* **140**(2), 1154 (2016).
- ⁴²M. Farhat, S. Guenneau, and S. Enoch, *Phys. Rev. Lett.* **103**(2), 024301 (2009).
- ⁴³N. Stenger, M. Wilhelm, and M. Wegener, *Phys. Rev. Lett.* **108**(1), 014301 (2012).
- ⁴⁴S. Cho, W. Yang, S. Lee, and J. Park, *J. Acoust. Soc. Am.* **139**(6), 3319 (2016).
- ⁴⁵D. Torrent, Y. Pennec, and B. Djafari-Rouhani, *J. Appl. Phys.* **116**(22), 224902 (2014).
- ⁴⁶A. Climente, D. Torrent, and J. Sanchez-Dehesa, *J. Appl. Phys.* **114**(21), 214903 (2013).
- ⁴⁷Y. Chen, J. Hu, and G. Huang, *J. Intell. Mater. Syst. Struct.* **27**(10), 1337 (2016).
- ⁴⁸R. Zhu, X. N. Liu, G. K. Hu, F. G. Yuan, and G. L. Huang, *Int. J. Smart Nano Mater.* **6**(1), 14 (2015).
- ⁴⁹X. S. Su and A. N. Norris, *J. Acoust. Soc. Am.* **139**(6), 3386 (2016).
- ⁵⁰X. Su, Z. Lu, and A. N. Norris, *J. Appl. Phys.* **123**(9), 091701 (2018).
- ⁵¹N. Yu, P. Genevet, M. A. Kats, F. Aieta, J.-P. Tetienne, F. Capasso, and Z. Gaburro, *Science* **334**(6054), 333 (2011).
- ⁵²A. Norris, *J. Vib. Acoust.* **140**, 034503 (2018).